Effect of Alkali and Alkaline Earth Metal Salts on Suppression of Lithium Dendrites

Johanna K. Stark Goodman* **and Paul A. Kohl****,z

Georgia Institute of Technology, School of Chemical and Biomolecular Engineering, Atlanta, Georgia 30332-0100, USA

Lithium dendrites are needle-like structures that form during the electrodeposition of lithium metal. These whiskers complicate the use of lithium metal as an anode in lithium batteries because they can puncture the separator and short circuit the battery. In addition, the large surface area and poor adhesion of the deposit contributes to loss of coulombic efficiency. The effect of alkali and alkaline earth metal ions on the morphology of electrodeposited lithium metal has been studied. Varying concentrations of alkali and alkaline earth metal ions were added to a 1 M lithium bis(trifluoromethanesulfonyl)imide (Li-TFSI) trimethylbutylammonium bis(trifluoromethanesulfonyl)imide (N_{1114}-TFSI) electrolyte. Lithium metal was electrodeposited from each electrolyte and examined ex-situ by scanning electron microscopy (SEM). Alkali metal ions, with the exception of sodium, had little or no effect on the deposited lithium morphology. However, alkaline earth metal ions at 0.05 M concentration significantly reduced the occurrence of dendrites. When the concentration of the alkaline earth metal ions was increased to 0.1 M, dendrites were completely eliminated and lithium was deposited in a sphere-like morphology. Energy dispersive X-ray spectroscopy (EDX) showed that no alkaline earth metals were found in the sphere-like deposits, suggesting that dendrite mitigation occurred through an adsorption mechanism.
 [DOI: 10.1149/2.0301409jes]

Manuscript submitted March 21, 2014; revised manuscript received May 21, 2014. Published May 31, 2014.

Lithium-ion batteries based on graphite anodes have been commercialized and used in mobile devices due to their high power and energy density. The graphite anode operates close to its theoretical capacity of 329 mAh/g. Thus, to increase the energy density of the overall battery, a new anode material must be developed. Reducing lithium ions on a substrate, rather than intercalating them into graphite, raises the specific capacity of the anode to 3861 mAh/g and is compatible with existing cathodes and future high-voltage cathodes.

Lithium-metal anodes suffer from low cycling efficiency for several reasons. First, the solid electrolyte interface (SEI) that forms on graphite anodes to protect the electrode from further reaction with the electrolyte, does not form as well on a metallic lithium surface. Second, the lithium metal anode undergoes extreme volume changes when going between the charged and discharged states, which can significantly disrupt the SEI during each cycle. Finally, when lithium metal is deposited on a substrate, such as during battery charging, lithium does not deposit as a dense, cohesive, planar layer, but rather deposits as needle-like structures, sometimes called dendrites, as shown in Figure 1.

Adding SEI forming additives and restricting the battery to shallow discharge cycles can mitigate some of these problems, however, these restrictions are not desirable. Vinylene carbonate (VC) has been shown to be a valuable additive for lithium metal batteries, yielding higher efficiencies and increased cycle life.[1,2] VC and other cyclic carbonates have been shown to form an SEI via ring-opening reactions that isolate the surface from the electrolyte.[3] Other organic molecules such as dimethyl carbonate, ethylene carbonate and fluorinated additives have also been used as additives to improve cycle life.[4,5] The high surface area associated with dendritic deposits compounds the problem of poor SEI formation because a greater quantity of SEI must be formed. During oxidation (battery discharge), it is possible that the base of the dendrite oxidizes prior to the tip, leading to loss of electrical contact with the substrate. In addition, if the dendrite bridges the gap between the anode and cathode, it can electrically short circuit the battery.[6] Recent in-situ studies on dendrite growth have shown that the needles can grow from the tip or extrude from the base, with both processes occurring in any given electrolyte.[7–12]

Lithium dendrite growth has previously been mitigated by physically confining the lithium metal behind a solid electrolyte,[13] however, this could lead to loss of contact in larger batteries as the lithium metal at the interface is shuttled to the cathode, causing delamination between the lithium anode, solid electrolyte, and current collector. There are also several reports of dendrite-free deposits in heavily fluorinated electrolytes[5,14,15] and the LiAsF6/dioxolane electrolyte.[16,17] A study in organic propylene carbonate/dimethyl carbonate (PC/DMC) electrolyte showed non-dendritic lithium deposition by addition of rubidium and cesium hexafluorophosphate to the electrolyte.[18] This was explained by an electrostatic shield mechanism where the adsorbed rubidium or cesium ions on the dendrite repel the lithium ions from the region of the dendrite. A low concentration of rubidium or cesium ions was required so that the deposition potential for rubidium or cesium was shifted to values negative of the lithium deposition potential, however, the actual deposition of rubidium and cesium was not examined experimentally. This is important because the assumed standard potentials may be different in the organic electrolyte. Further, restricting the deposition potential for lithium (i.e. potential the anode is charged) would result in low charging currents.

In ionic liquid systems, the suppression of dendritic growth of lithium has been studied by co-depositing a second metal with lithium from bis(trifluoromethanesulfonyl)imide (TFSI) and chloroaluminate ionic liquid electrolytes.[11,19] A non-dendritic, sphere-like lithium morphology was achieved through the co-deposition sodium with lithium. The remaining alkali TFSI salts have been synthesized and their reduction potentials characterized, opening the door for their study in conjunction with lithium. Potassium, rubidium, and cesium can be reversibly deposited at potentials negative of lithium deposition in TFSI-based electrolytes, making co-deposition feasible.[20]

The group 2 alkaline earth metals, of which magnesium has been considered for battery applications, are of interest. Magnesium has been more difficult to deposit than lithium because the surface films formed on magnesium are more insulating and are not as ion conducting as their lithium counterparts.[21] Reversible magnesium deposition has been achieved in from Grignard based solutions and some ionic liquids electrolytes.[22–26] The remaining alkaline earth metals, calcium, strontium and barium, have not been studied alone or as additives in lithium deposition. Calcium, strontium, and barium are used in phosphate and carbonate coatings for biocompatibility, but these coatings are formed by electrochemically assisted deposition, not a direct reduction of the metal. Nitrates are electrochemically reduced lowering the pH at the substrate, which causes phosphates and carbonates of these metals to precipitate.[27–30]

Ionic liquids (ILs) provide a suitable electrolyte system to test the effects of alkali and alkaline earth metal ions on the lithium metal anode. Reversible lithium reduction/oxidation has been shown by

*Electrochemical Society Student Member.
**Electrochemical Society Fellow.
zE-mail: Kohl@gatech.edu

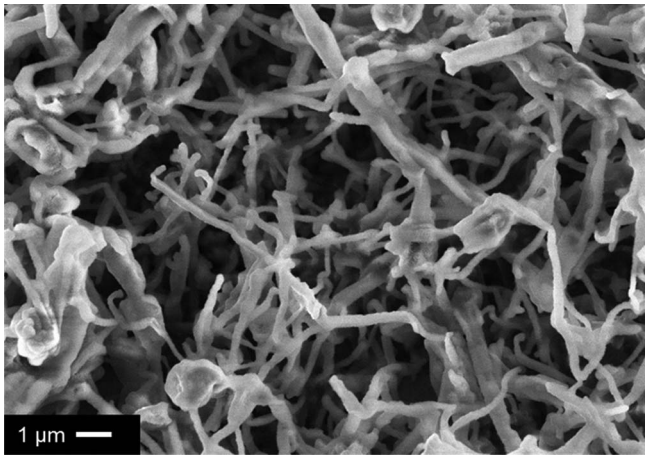

Figure 1. Lithium deposited from a 1 M Li^+ electrolyte at −0.3 V for 500 s. Lithium is dendritic for a wide range of potentials and times.

multiple groups.[11,20,26,31] The TFSI-based ionic liquid system is also compatible with remaining alkali metals.[20] This work explores alkali and alkaline earth TFSI salts as additives to lithium electrolytes with the goal of changing the dendritic morphology of the lithium metal deposit.

Experimental

The ionic liquid, trimethylbutylammonium bis(trifluoromethanesulfonyl)imide (N_{1114}-TFSI), was purchased from Iolitec (99%) and used for all experiments. Lithium bis(trifluoromethanesulfonyl)imide (Li-TFSI), the lithium salt with the matching anion, was purchased from Wako. The alkali and alkaline earth TFSI salts were either purchased or synthesized via reaction of the metal hydroxide and trifluoromethanesulfonimide (H-TFSI, Wako). Barium bis(trifluoromethanesulfonyl)imide (Ba-$TFSI_2$), magnesium bis(trifluoromethanesulfonyl)imide (Mg-$TFSI_2$), and calcium bis(trifluoromethanesulfonyl)imide (Ca-$TFSI_2$) were purchased from Sigma Aldrich. The sodium, potassium, rubidium, and cesium salts were synthesized by reaction of the metal hydroxide with a stoichiometric amount of H-TFSI and then adjusting to neutral pH (Equation 1). The solution was gently heated to remove water and then dried under vacuum for 12 h. Strontium bis(trifluoromethanesulfonyl)imide (Sr-$TFSI_2$) was synthesized in a similar manner as shown in Equation 2. Electrolytes were made by dissolving the appropriate amount of Li-TFSI and additive-TFSI salt in N_{1114}-TFSI ionic liquid. The electrolytes were dried under vacuum for one to two days before use.

$$MOH + HTFSI \rightarrow MTFSI + H_2O \quad [1]$$

$$M(OH)_2 + 2\,HTFSI \rightarrow MTFSI_2 + 2\,H_2O \quad [2]$$

The electrochemical studies were performed in an argon filled glove box (Vacuum Atmospheres) with a water content below 0.04 ppm. A Perkin Elmer Parstat 2263 with PowerSuite software was used to carry out all electrochemical experiments. Cyclic voltammograms (CVs) were conducted in a two electrode cell with a stainless steel type 316 working electrode and a lithium reference and counter electrode. The lithium metal counter generally provides a stable potential so that it can be used as a reference electrode. Isolated experiments with a separate lithium reference electrode (three electrode cell) were conducted and no change in the voltammograms was observed. In electrolytes with different ions, the counter electrode served as a pseudo-reference because the foreign ion could change the rest potential of the counter electrode. Thus, the reference potential may be slightly different in the foreign metal electrolytes and the current-voltage curves are plotted separately. A potential scan rate of 0.01 V/s was used to generate CVs. A Zeiss Ultra 60 scanning electron microscope (SEM) was used for imaging samples prepared in the same configuration. SEM samples were held at a constant potential for 500 s and then washed with anhydrous dimethyl carbonate (DMC, anhydrous, ≥99% Sigma-Aldrich) to remove the viscous ionic liquid. Elemental analysis was done with energy dispersive X-ray spectroscopy (EDX) using Oxford Instruments X-Sight column and INCA software.

The coulombic efficiency of lithium deposition and re-oxidation in the different electrolytes was evaluated by cyclic voltammetry. By integrating under the reduction and re-oxidation peaks, the charge passed for each process can be calculated. The beginning of the reduction was defined as the rise in current associated with the reduction peak. A coulombic efficiency can then be calculated by dividing the charge associated with the re-oxidation by the charge associated with reduction.

Results

The effect of addition of metal ions on the deposition of lithium metal was investigated. The added cation can have one of several affects including co-depositing, changing the electrolyte conductivity, and changing the electrical double layer (EDL). When the Li-TFSI dissolves in N_{1114}-TFSI, a clear, viscous electrolyte is formed. A constant potential deposition yields a deposit, shown in Figure 1, where the surface is dominated by dendrites. The high surface area of the dendrites complicates surface passivation via a solid electrolyte interface (SEI) necessary for stable battery operation. In addition, the dendrites can break off or oxidize at the base causing loss of active material from the electrode surface.

The group 1 alkali metals ions investigated were sodium, potassium, rubidium and cesium. Previously, sodium ions have been shown to co-deposit with lithium forming a non-dendritic, sphere-like deposit.[11,19] The reduction potential of the remaining alkali metal ions were experimentally measured in pyrrolidinium TFSI ionic liquid by Wibowo et al.[20] The pyrrolidinium TFSI ionic liquid is similar to the quaternary ammonium TFSI ionic liquid used in this work so it is reasonable to assume that the potentials will follow the same trend. While sodium reduces 0.184 V positive of lithium, the remaining alkali metals reduce at potential negative of lithium, even though their standard potentials are positive of lithium. Potassium reduces −0.109 V vs. Li/Li+, Rubidium at −0.117 V, and cesium at −0.122 V. This means that to observe a co-deposit of lithium with these three metals, potentials more negative than these values, corrected for concentration by the Nernst equation, are necessary assuming under-potential deposition does not occur. Each alkali metal was first tested in a 0.1 M solution in N_{1114}-TFSI without lithium ions being present. Lithium metal was used as a pseudo-reference electrode in these experiments. Due to the different species in the electrolyte, the reference potential may differ slightly from electrolyte to electrolyte. Nevertheless, the electrolyte reduction potential can serve as a common guide. The voltammetry with 0.1 M Na^+ is shown in Figure 2, while voltammetry with 0.1 M K^+, Rb^+, and Cs^+ is shown in Figures 3a–3c respectively. With the exception of lithium, sodium exhibited the most reversible behavior with a clearly defined reduction peak starting at 0.09 V. On the reverse scan, Na oxidation began at 0.16 V. The overpotential observed is likely due to the nucleation effect of plating a metal on a foreign surface and has been observed previously.[20,32,33]

In contrast, no reduction of potassium was observed on the stainless steel electrodes, as seen in Figure 3a. Two peaks at 0.9 V and 0.4 V were observed on the first cycle but not observed on subsequent cycles, suggesting a one-time surface modification to the stainless steel, rather than an irreversible deposit. While reversible potassium deposition from TFSI-based ionic liquids has been observed on nickel and tungsten electrodes,[20,34] another attempt from chloroaluminate ionic liquid failed on tungsten but succeeded on mercury.[35] Based on the different results for potassium deposition, reduction is more surface dependent than the other metal ions.

Wibowo et al. reported that rubidium and cesium were reduced near the potential limit of the ionic liquid used here, which is ca.

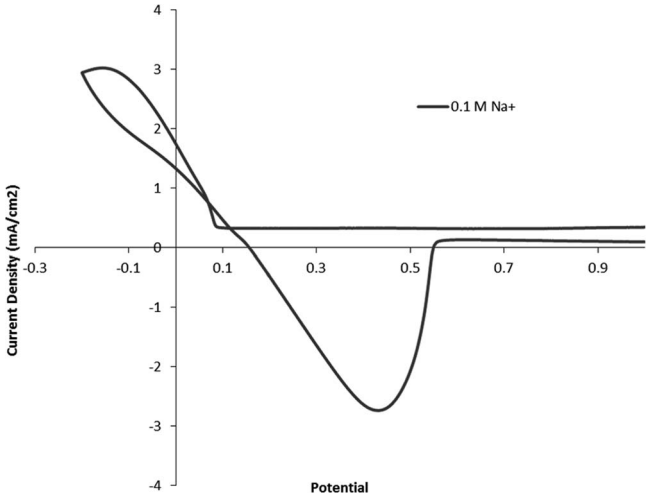

Figure 2. The CV of 0.1 M Na^+ electrolyte shows reduction starting at 0.09 V. Sodium was the only alkali metal other than lithium, to show clean reversible reduction and oxidation peaks.

−0.35 V vs. Li/Li^+.[20] The CV of a 0.1 M Rb^+ electrolyte versus a lithium pseudo-reference electrode is shown in Figure 3b, where the electrolyte decomposition occurs at −0.3 V. This is the expected potential and acts as an internal reference. Two reduction peaks were observed on the forward scan at 0.9 V and 0.4 V. Constant potential experiments were performed to investigate the origin of the peaks. The potential step experiments showed that little to no metal was deposited on the substrate in these two potential regions. The lack of a deposit suggests that the products from these peaks are soluble or the result of a surface modification rather than being an electrodeposit. The peaks decreased in height over multiple voltage scans. An oxidation peak was observed at −0.25 V, which was identified as the reoxidation of rubidium. Pourous rubidium deposit was observed in a separate 500 s potential step to −0.4 V. The reduction of Rb^+ is very close

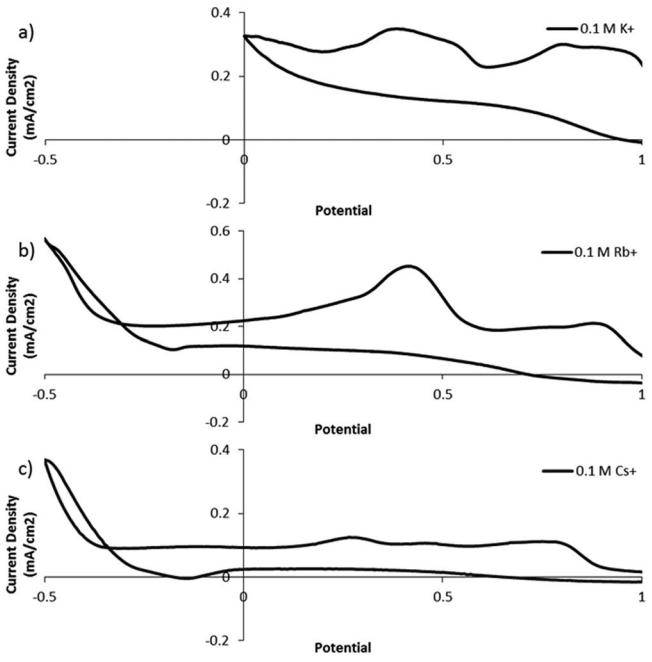

Figure 3. CV of a) potassium, b) cesium, and c)rubidium only electrolytes. Potassium showed no reversible behavior. Small reduction peaks are visible for rubidium and cesium confirming some reversible behavior but the electrolyte stability window prevents a true reversible deposit.

to the decomposition potential of the electrolyte. This results in poor coulombic efficiency for reduction and re-oxidation of rubidium.

A CV was performed in a 0.1 M Cs^+ electrolyte (vs. Li metal pseudo-reference electrode) and is shown in Figure 3c. The electrolyte decomposition at −0.3 V serves as an internal reference. Cesium displayed several small oxidation peaks between 0.2 V and 1.0 V. When the electrode was held at 0.5 V, well within the range of these peaks, SEM and EDX showed sparse nanometer-sized cesium-rich particles on the surface but the CV shows no electrochemical evidence that their formation is reversible. Subsequent CV cycles showed that these peaks decreased in height, but did not disappear altogether. This indicates that they are likely caused by reactions with the pristine surface, rather than a bulk process. A small oxidation peak was observed at −0.29 V for cesium. To help identify the origin of this peak, the electrode was poised at −0.4 V for 500 s. A porous deposit with high cesium content was observed by SEM. This indicates that the small oxidation peak at −0.29 V is due to metallic cesium. The peak is small because the potential at which cesium is deposited also coincides with electrolyte decomposition as a competing reaction. In addition, some cesium could have been lost due to reaction with the electrolyte after the metal was formed.

The electrolytes containing 0.1 M concentration of K^+, Cs^+, Rb^+ described above were made 1.0 M Li^+, in addition to the 0.1 M alkali metal. Figure 4 shows the cyclic voltammograms recorded for these new electrolytes, which now contain 1 M Li^+ and 0.1 M alkali metal ions. Each electrolyte showed peaks for lithium deposition and stripping. The overpotential for the Li redox process remained −0.075 V regardless of which metal was added indicating a minimal effect of the foreign metal ions on the Li/Li^+ couple. Rather, the addition of the second metal ion affected the peaks between 0 V and 1 V, which are associated with surface, rather than bulk, processes. On stainless steel, lithium showed two peaks at 1.3 V and 0.4 V on the forward scan, prior to the reduction of lithium ions to metallic lithium. The first peak at 1.3 V is an irreversible surface process that only appears on the first cycle. It is likely an initial surface film that forms on the substrate involving Li^+ ions, as the peak does not appear for the neat ionic liquid. By reversing the scan direction at 0 V, prior to Li^+ reduction, the second peak at 0.4 V can be paired with the peak at 1.3 V on the reverse scan. This set of peaks remained constant over multiple cycles and is likely the reversible intercalation/de-intercalation of lithium into the surface oxide present on stainless steel. Allowing the potential scan to go negative of 0 V vs. Li/Li^+ shows that lithium reduction begins at −0.075 V and the re-oxidation peak appears on the reverse scan starting at 0 V. The coulombic efficiency associated with lithium ion reduction and re-oxidation is 65%, which is lower than what can be

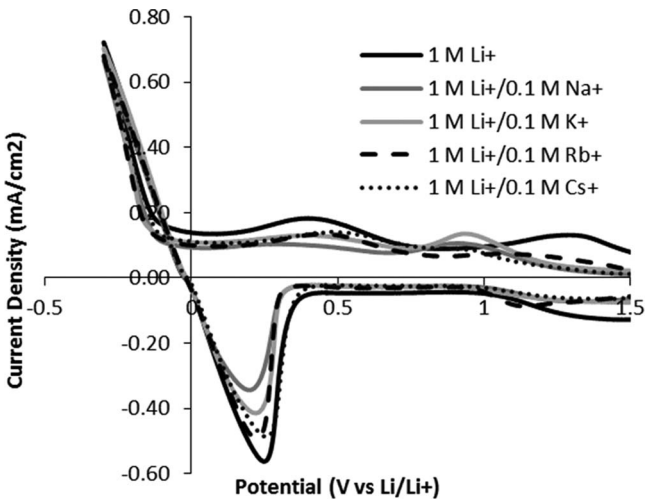

Figure 4. Cyclic voltammograms of lithium electrolytes with 0.1 M alkali metal ions.

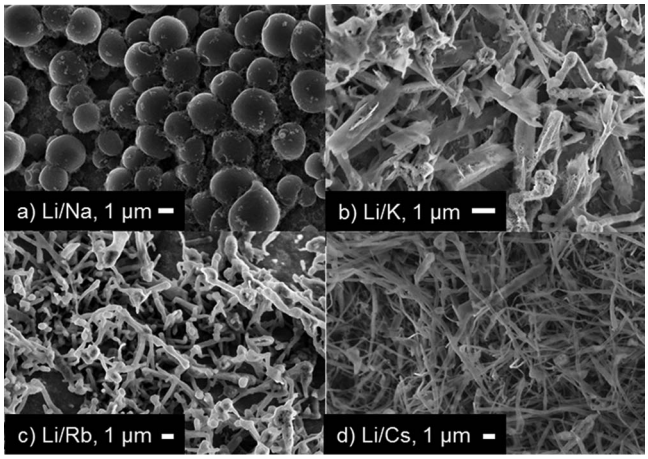

Figure 5. SEM images of lithium deposits from 1 M Li^+ electrolyte with 0.1 M alkali metal ions. Substrate was held at a) −0.15 V, b) −0.3 V, c) −0.4 V, and d) −0.4 V for 500 s. Potentials were chosen based on the different overpotentials for each electrolyte and the ability to deposit the alkali metal ion at that potential.

achieved in an actual battery because deposition on a foreign surface, here stainless steel, affects the charge passed on each cycle. In a commercial cell, a shallow cycling method could be used to avoid this problem.[36,37] In addition, the background current associated with the surface oxide intercalation lowers the calculated efficiency.

The addition of sodium ions to the lithium ion containing electrolyte shifted the first irreversible peak at 1.3 V to 0.9 V. As described above, this peak did not appear on the second cycle pointing to a one-time surface modification. From previous work, it has been shown that lithium and sodium can be co-deposited to form a non-dendritic deposit.[11,19] The lithium/sodium co-deposit consisted of many spheres with at least one indentation on the surface. This morphology is shown in Figure 5a where 1.3 C/cm^2 was passed over 5000 s. This co-deposit was studied in detail in a previous paper.[11] The coulombic efficiency for the deposition and re-oxidation of the lithium/sodium system was calculated to be 44%. While it is possible for the absence of dendrites to lead to an increase in the coulombic efficiency, the coulombic efficiency of sodium from the CV results was only 41%. This relatively poor redox efficiency for sodium appears to be the cause of the lower coulombic efficiency for the lithium/sodium system.

No metal was electrodeposited from the potassium-only electrolyte, thus no co-deposit of lithium and potassium was expected. A CV of the 1.0 M Li^+/0.1 M K^+ electrolyte showed two reduction peaks prior to lithium ion reduction, followed by lithium re-oxidation on the reverse scan. The surface related peak that appears at 1.3 V in the lithium-only electrolyte has again been shifted to 0.9 V, as in the lithium/sodium electrolyte. This peak appeared only on the first cycle, indicating an initial surface reaction, rather than a bulk process. The peaks related to lithium intercalation into the surface oxide, at 0.4 V on the forward scan and 1.3 V on the reverse scan, were not affected by the addition of potassium. The coulombic efficiency for lithium reduction and re-oxidation was 51%. The lithium/potassium deposit exhibited a flake-like morphology, as shown in Figure 5b where 0.3 C/cm^2 of charge was passed during a 500 s at −0.3 V vs. Li/Li^+. The flakes were 1 µm wide and 2–3 µm long. The edges of the larger flakes and smaller platelets give the deposit a crystalline appearance. Individual flakes look detached from the substrate as well as each other and exhibited the same high surface area that is detrimental to cycling efficiency.

The potential scans changed little when either Rb^+ or Cs^+ (0.1 M) were included in the 1.0 M Li^+ electrolyte. The coulombic efficiency for the Rb^+ and Cs^+ containing electrolytes was 57% and 61%, respectively. The characteristic peaks seen in lithium-only electrolytes remained unchanged as shown in Figure 4. Cesium and rubidium were electrodeposited at −0.4 V vs. Li/Li^+ resulting in ∼0.4 C/cm^2 over 500 s for both cases (Figure 5). This potential was chosen to maximize the possibility of a co-deposit. Images of deposits generated at more positive potentials (lower current and less C/cm^2) looked qualitatively similar to those at more negative potentials. The dendritic lithium deposit morphology in the presence of Rb^+ or Cs^+ was unchanged even when material was deposited at −0.4 V, a potential where the metal ions are reduced from their individual electrolytes. Figures 5c and 5d show that dendrites from the lithium/rubidium and lithium/cesium electrolytes have a diameter of 0.2 to 0.5 µm, similar to the dendrites of a lithium-only deposit shown in Figure 1. The dendrites were entangled, constant-diameter needles that had a high surface area and poor adhesion to the stainless steel substrate. The EDX results showed no cesium or rubidium present in the electrodeposit, thus only the Li^+ and IL reduction occurred.

The survey study of 0.1 M alkali/1 M lithium electrolytes suggests that in order to prevent dendritic growth, the alkali metal ion should be co-deposited. In this IL, co-deposition was only possible with sodium because the reduction potential for cesium and rubidium were too close to of the decomposition potential of the IL.

The group 2 alkaline earth metal ions, Mg^{2+}, Ca^{2+}, Sr^{2+} and Ba^{2+}, were added to the 1 M Li^+ electrolyte to examine their effect on the form of the lithium electrodeposit. The lower solubility of the divalent ions increased the viscosity of the IL. Electrolytes containing 0.1 M Mg^{2+}, Ca^{2+}, Sr^{2+} or Ba^{2+} yielded milky-white solutions compared to the clear solutions formed with the alkali metal salts. CVs for each of these electrolytes are shown in Figure 6. The morphology resulting from these electrolytes was examined by polarization to −0.3 V vs. Li/Li^+ for 500 s. This resulted in 0.2–0.3 C/cm^2 depending on the electrolyte.

Because of the interest in a magnesium metal battery, a 0.1 M Mg^{2+} electrolyte was tested for Mg deposition, however, no CV peaks or deposit were observed. Although magnesium metal does not deposit from the Mg-only electrolyte, Mg^{2+} had a dramatic influence on the form of the lithium deposit. The magnesium salt also appeared to increase the voltage stability window of the IL. As shown in Figure 6, a CV of a 1 M Li^+/0.1 M Mg^{2+} electrolyte showed no sharp current rise at −0.35 V, where the ionic liquid is usually reduced. Instead, a gradual rise in current was observed with a much reduced slope. The gradual rise at −0.4 V is likely due to electrolyte reduction. None of the above-mentioned peaks associated with lithium appeared in the scan. Lithium ion reduction was observed at a lower 0.05 M Mg^{2+} concentration followed by re-oxidation, however, the overpotential for lithium ion reduction was −0.4 V, which also led to electrolyte reduction. The coulombic efficiency, based on the reduction and oxidation peaks,

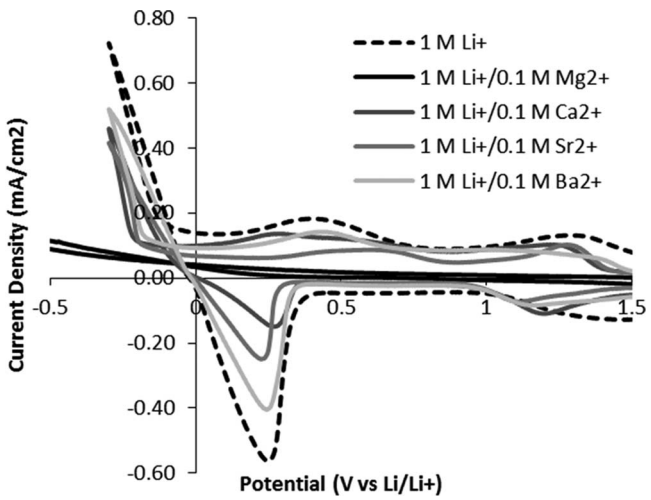

Figure 6. Cyclic voltammograms of lithium electrolytes with 0.1 M alkaline earth metal ions.

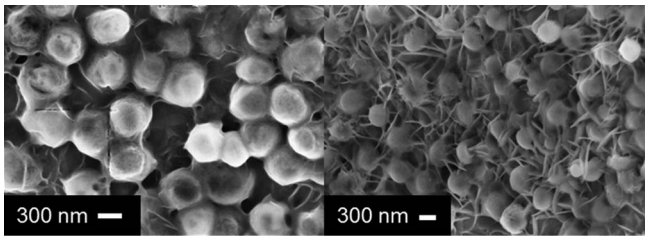

Figure 7. Lithium deposit from a 1 M Li^+/0.05 M Mg^{2+} electrolyte at −0.5 V for 500 s.

was only 17% because of the extreme polarization required to reduce lithium ions. The electrodeposit had the appearance of spheres covered by a web-like material, as shown in Figure 7. The webbing was shown to be carbonaceous by EDX analysis and likely consists of the products from electrolyte reduction. The spheres mostly disappeared after re-oxidation of the lithium at 1 V, showing that they were indeed lithium metal.

The addition of Ca-$TFSI_2$ to a 1 M Li^+ electrolyte did not suppress lithium reduction and re-oxidation currents to the same extent as magnesium salt. The current density observed with Ca^{2+} in the electrolyte was lower than for the lithium ion only electrolyte. The CV shown in Figure 6 shows a clear lithium reduction and re-oxidation current in the Ca^{2+} containing electrolyte, although the overpotential for Li^+ reduction increased to 0.2 V (the reduction current started at −0.2 V vs. Li/Li^+) compared with the lithium-only electrolyte, where the overpotential was 0.08 V. The lithium metal oxidation peak was smaller than the reduction peak, yielding a coulombic efficiency 31% for the lithium/calcium electrolyte. The sloping onset of the oxidation peak also indicates that an overpotential is also associated with the oxidation. Lithium was deposited from electrolytes with a Ca^{2+} concentrations of 0.05 M and 0.1 M. The lithium concentration was held constant at 1 M Li^+ (Figure 8) in both cases. Deposits from the 0.05 M Ca^{2+}/1 M Li^+ electrolyte showed some dendritic growth, however, a majority of the particles were dimpled spheres, similar to the sodium case. The deposit was fully non-dendritic when the Ca^{2+} concentration was raised to 0.1 M. An EDX element map of this deposit showed that no calcium was deposited on the substrate. Despite the similar appearance to the lithium/sodium deposit, this deposit, originating from the lithium/calcium electrolyte, contained no calcium within the detection limits of EDX. Thus, the dendrite blocking mechanism appears to occur via an adsorption mechanism, rather than by co-deposition. Close inspection of the deposit shows a roughened substrate with fibrous material between the dimpled spheres. This could be decomposed electrolyte, which results in the lower efficiency.

The addition of 0.1 M Sr^{2+} or Ba^{2+} to the IL electrolyte showed similar behavior to that of Ca^{2+}. Based on the CV in Figure 6, the coulombic efficiency was 43% for the strontium and 65% for the barium containing electrolyte. The current density was lower for these two electrolytes compared to the lithium-only electrolyte, but was higher than the Ca^{2+} case. The deposits produced from the lithium/strontium and lithium/barium electrolytes (i.e. 0.05 M and 0.1 M concentrations of Sr^{2+} or Ba^{2+}) with the 1 M Li^+ were examined. The images,

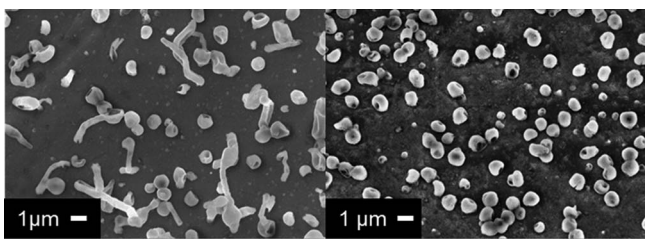

Figure 8. Lithium deposited at −0.3 V for 500 s from a (left) 1 M Li^+/0.05 M Ca^{2+} electrolyte and (right) 1 M Li^+/0.1 M Ca^{2+} electrolyte.

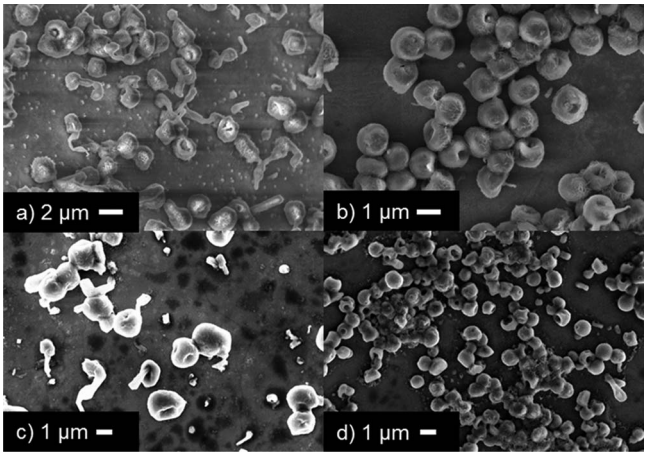

Figure 9. Deposits from electrolytes held at −0.3 V for 500 s. a) 1 M Li^+/0.05 M Sr^{2+}, b) 1 M Li^+/0.1 M Sr^{2+}, c) 1 M Li^+/0.05 M Ba^{2+}, d) 1 M Li^+/0.05 M Ba^{2+}.

Figure 9, show the deposit morphology for the four cases. At 0.05 M, a significant change in the deposit morphology was observed compared to the lithium-only deposit in Figure 1. The effect of Ba^{2+} and Sr^{2+} on the deposit was similar to the effect of Ca^{2+} ions. Most of the deposit was composed of dimpled spheres with some dendrites. When the concentration was increased to 0.1 M, nearly all deposited material was in the form of dimpled spheres. Only an occasional dendrite was observed. The same fibrous material was observed on the deposit from the lithium/calcium electrolyte was observed on the deposit from the lithium/strontium or lithium/barium electrolytes, although to a lesser degree. EDX analysis did not show any trace of strontium or barium in the sample, suggesting that like the calcium and magnesium cases, dendrite suppression occurred at the electrode/electrolyte interface rather than by significant co-deposition.

The doubly charged alkaline earth ions behaved differently from the singly charged alkali ions. While the alkali metals required co-deposition to form non-dendritic lithium, alkaline earth metals prevented dendritic growth without being codeposited, at least to the sensitivity of the experiments performed here. This is possibly due to a change in the electrical double layer that forms upon polarization or an inhibition of the surface to electron tranfer. The electrical double layer (EDL) in an ionic liquid differs from that of an organic electrolyte because the charge density is significantly higher, resulting in a multilayered structure. In conventional solutions, salts are dissolved through the formation of a neutral solvent shell around the ions. Compact and diffuse layers form in the presence of a charged surface to balance that charge. Models for the double layer in aqueous systems are based around dilute solutions but ionic liquids do not follow these assumptions.[38,39] Molecular dynamic simulations have shown that distinct anion and cation layers form at the electrical interface of an IL and a charged surface.[40] The first layer consists of the large N_{1114}^+, Li^+, and double charged alkaline earth cations. Next distinct layer will consist of $TFSI^-$, the only anion in the system. Ionic liquid double layers consist of multiple alternating ion layers, making the charge distribution near the surface more complex.[41] Because the doubly charged alkaline earth cations are each associated with two $TFSI^-$ anions, this layer will be bulkier and/or denser than in an electrolyte without the additional anions. This could hinder lithium transport to the surface during plating, essentially negating the preferential growth on possible dendritic sites.

Discussion

Electrodeposited lithium dendrites are a major safety concern for lithium metal and lithium intercalation anodes. Potential short circuits from dendrites growing across the separator forming a bridge to the

cathode could result in thermal run-away, thus understanding how dendrites grow and finding methods to prevent them is critical. In-situ observations shown that dendrites grow from the tip as well as from the base. Growth at the tip occurs electrochemically. For a whisker to form, the deposition rate at the tip must be much higher than on the sidewalls. A non-uniform current density, possibly caused by higher exchange currents on specific crystal faces, is thus inherent in dendritic growth. Base growth is thought to be an extrusion mechanism where pressure builds within the metal under the SEI, causing the soft lithium to extrude along grain boundaries. Tip growth can be prevented by mitigating the non-uniform current density that causes dendrites. The co-deposition of a second metal can alter the exchange current for lithium deposition, thus limiting the run-away dendritic growth. Alternatively, electrostatic repulsion of lithium ions through the absorption of cations has also been proposed as a dendrite-limiting mechanisms.[18] Mitigation of extrusion based growth would require a change to the material properties of the deposit, such as increasing creep resistance. The SEI layer plays a crucial role in both tip growth and base growth mechanisms. A dense SEI layer can inhibit transport to the tip, thus limiting the deposition rate at that location through concentration polarization. For growth by extrusion, the mechanical properties of the SEI layer contribute to the pressure buildup that causes extrusion.

Additives to the electrolyte can have a variety of effects on the Li/electrolyte interface. The most common additives are SEI formers, such as EC or VC, whose role is to form a protective SEI layer over the anode. The chemical changes in the SEI layer upon addition of these additives are well documented. A dense, protective SEI can increase the coulombic efficiency of the anode by limiting the transport of fresh electrolyte to the reactive lithium metal. It is not inconceivable however, that the SEI could also affect the morphology of the deposit by limiting the flux of ions to be deposited to the surface or by creating a mechanical barrier to dendritic growth. The additives used in this study are metal salts, which exist in the electrolyte as ions and can become part of the electrical double layer. The ions can adsorb on the surface, thus changing lithium ion transport to that surface. Ion reduction followed by crystal nucleation (i.e. electrodeposition) is a multistep process where ions must first diffuse to the surface, including through the SEI layer, adsorb, undergo electron transfer creating the adatom, and finally assimilate into the lattice. An adsorbed ion layer could hinder the deposition process because of electrostatic effects or block reduction/nucleation sites inhibiting the overall process. Metal ions can also deposit from the electrolyte to form a co-deposit with lithium. The co-deposited metal would have a different exchange current density or could physically block dendrite growth because of the lattice mismatch between the two different metals.

The group 1 alkali metals were targeted as additives that would co-deposit with lithium. Reduction of sodium, potassium, rubidium, and cesium ions has been previously shown using a pyrrolidinium-TFSI ionic liquid. Wibowo et al. measured the reduction potentials and found that sodium ions reduce positive of lithium, but potassium, rubidium and cesium reduce negative of lithium. While the potentials themselves will not be the same given our slightly different ionic liquid, the same trend holds. When considering a co-deposit the deposition potential plays a significant role in whether such a co-deposit would form. A summary of observations at various potentials is detailed in Table I.

Sodium ions showed the most reversible behavior for reduction/oxidization from the N_{1114}-TFSI ionic liquid. Adding Na-TFSI to the electrolyte in small concentrations resulted in a dimpled-sphere shaped deposit. This is likely to occur because sodium would electrodeposit on the high current density sites where lithium dendrites would have originated. Foreign sodium atoms on these sites inhibit the high growth rate because the site no longer has the original high exchange current. Also, lithium and sodium do not alloy so that the presence of sodium would change the nature of the surface. Although it was not observed here, a lithium/sodium co-deposit could also prevent dendrite base growth (extrusion process) because the properties of the deposit would be different. Lithium by itself is a soft metal susceptible to creep. The addition of sodium could change the hardness and creep character of the deposit, potentially preventing extruded dendrites.

Table I. Summary of morphologies observed from 1 M Li^+/0.1 M group 1 electrolytes.

	−150 mV vs Li/Li^+	−300 mV vs Li/Li^+	−400 mV vs Li/Li^+
Na	Shown non-dendritic up to 5000 s (1.5 C/cm^2)		
K		Flake-like	
Rb	dendritic	dendritic	Dendritic, no Rb observed even though the potential is sufficient for reduction
Cs	dendritic	dendritic	Dendritic, no Cs observed even though potential is sufficient for reduction

Potassium ions were not reduced on stainless steel and their addition to the lithium ion containing electrolyte yielded a flake-like deposit, however dendrites still occurred.

Rubidium and cesium ions can be reduced at very negative potentials close to the electrolyte decomposition potential, thus a potential of −0.4 V vs. Li/Li^+ was used in an attempt to obtain a co-deposit. As summarized in Table I, no co-deposit was observed and the morphology remained dendritic. A non-dendritic co-deposit may still possible with cesium or rubidium ions if a more stable ionic liquid were found and the concentration of cesium or rubidium ions was increased. This would allow for a more negative deposition potential where cesium and rubidium ions could be reduced. Ding et al. proposed a mechanism whereby a foreign ion that would deposit 0.05 – 0.1 V negative of lithium prevents dendrites, and showed this with cesium ions in an organic electrolyte. The same effects were not observed in this ionic liquid electrolyte, regardless of potential applied as shown in Table I.

The addition of small amounts of group 2 alkaline earth ions had a dramatic effect on the lithium metal deposit morphology. These ions were not electrodeposited from the ionic liquid, rather, they served as inhibitors and their effects were highly dependent on concentration. Table II summarizes the effect of adding varying concentrations of group 2 ions to a 1 M Li electrolyte.

All alkaline earth metals inhibited dendritic growth; however, lower current densities and increased overpotentials were observed. Although their standard potentials are 0.1 – 0.3 V vs. Li/Li^+, well within the potential window of the IL, individual testing (0.1 M concentration without lithium) showed that none of the alkaline earth metals deposited from the ionic liquid electrolyte. The reduction potential of these ions could be more negative in this particular liquid and salt, possibly because a necessary intermediate for the two electron transfer cannot form or the metal ion is bound too tightly.

Table II. Summary of morphologies observed from 1 M Li/x M group 2 electrolytes.

	0.05 M	0.1 M
Mg	Granular Li at high over-potentials	All redox reactions completely suppressed
Ca	Slightly dendritic, but mostly granular, very low current density	Non-dendritic, very low current density
Sr	Slightly dendritic, but mostly granular	Non-dendritic
Ba	Slightly dendritic, but mostly granular	Non-dendritic

While alkaline earth metal ions did not deposit on their own, their addition to a 1 M Li^+ electrolyte affected both the coulombic efficiency and the morphology of the lithium deposit. Given the same concentration, the coulombic efficiency of lithium increased with increasing size of the additive ion, although not above the coulombic efficiency for an additive-free electrolyte. The deposit morphology can have a large impact on the coulombic efficiency, given that the surface area influences how much SEI will be formed. Lithium metal can also be lost due to dendrites being oxidized at the base of the deposit, and thus losing contact with the electrode. In the case of alkaline earth metal ions, very few dendrites were observed and the morphology of the deposit was similar for the different additive ions. The resulting trend in the coulombic efficiency was likely due to a parasitic reaction between the fresh lithium deposit and the electrolyte, with the extent of reaction varying between the additive ions.

Co-deposition with lithium was not observed, thus it is hypothesized that upon negative polarization of the substrate, the positively charged alkaline earth metal ions adsorb on the substrate surface. The alkaline earth salts are bulky due to their larger size and two $TFSI^-$ counter anions so diffusion through the SEI layer would more difficult than for Li^+ with its single counter ion. The doubly charged alkaline earth ions likely remain outside the SEI layer as part of the electrolyte rather than the deposited structure, though detection by EDX would be unlikely if they were present in the SEI in small amounts. The alkaline earth salts are thought to impede diffusion to the surface, adding an additional rate-limiting step. The growth rate at the dendrite tip is much higher than the growth rate on the sidewalls giving the dendrite its needle-like shape. The addition of a rate limiting step before reduction would mitigate this accelerated growth rate, resulting in a uniform current density and non-dendritic deposit.

Magnesium ions suppressed the reduction of lithium ions and the electrolyte, as shown by the lower currents during voltammetry. This was not due to an electrochemically formed surface film, because no such current peak was observed in the CV. The decrease in current density seen with both lithium ion reduction and electrolyte reduction is consist with the absorption of an inhibitor rather than a lithium-specific process because the inhibition occurred over both processes on a stainless steel substrate, rather than only on a lithium substrate. Moving down the periodic table, suppression of the lithium redox reaction lessened with the (individual) addition of Ca^{2+}, Sr^{2+}, and Ba^{2+}. It is noted that the larger ions would have increased difficulty in diffusing through the SEI to the lithium surface and likely do not affect the structure or composition of the SEI. The overpotential associated with lithium ion reduction decreased from 0.20 V for Sr^{2+} to 0.14 V for Ba^{2+}, whereas a lithium-only electrolyte showed an overpotential of 0.09 V vs. Li/Li^+. This increased overpotential also supports the hypothesis of inhibition through adsorption because such an effect would make the surface more difficult for lithium to nucleate on. Given the trend in current density and overpotential, Mg^{2+} adsorbs the strongest, followed by Ca^{2+}, Sr^{2+}, and Ba^{2+}.

A concentration-dependent dendrite suppression was observed with calcium, strontium, and barium resulting in a deposit with a mix of spheres and dendrites when the ions were present at a lower concentration, and spheres only for the higher ionic concentrations. If an adsorption of an ion were to add a rate-limiting step, the concentration of foreign ions would control the extent of that step. A higher concentration of alkaline earth ions in the bulk leads to denser coverage of adsorbed ions on the surface, resulting in greater diffusion inhibition. A change in morphology was observed when the concentration of the additive was at least 0.05 M. Complete dendrite suppression occurred as a result of inhibited lithium ion transport to the surface at a critical concentration of 0.1 M.

Acknowledgments

The authors gratefully acknowledge the financial support of the US Army, contract US001-0000245070.

References

1. H. Ota, Y. Sakata, Y. Otake, K. Shima, M. Ue, and J. Yamaki, *J. Electrochem. Soc.*, **151**, A1778 (2004).
2. H. Sano, H. Sakaebe, and H. Matsumoto, *J. Electrochem. Soc.*, **158**, A316 (2011).
3. X. J. Wang, H. S. Lee, H. Li, X. Q. Yang, and X. J. Huang, *Electrochem. Commun.*, **12**, 386 (2010).
4. R. Mogi, M. Inaba, S.-K. Jeong, Y. Iriyama, T. Abe, and Z. Ogumi, *J. Electrochem. Soc.*, **149**, A1578 (2002).
5. H. Ota, X. Wang, and E. Yasukawa, *J. Electrochem. Soc.*, **151**, A427 (2004).
6. M. Rosso, C. Brissot, A. Teyssot, M. Dollé, L. Sannier, J.-M. Tarascon, R. Bouchet, and S. Lascaud, *Electrochim. Acta*, **51**, 5334 (2006).
7. C. Brissot, M. Rosso, J.-N. Chazalviel, and S. Lascaud, *J. Power Sources*, **81**, 925 (1999).
8. K. Nishikawa, T. Mori, T. Nishida, Y. Fukunaka, M. Rosso, and T. Homma, *J. Electrochem. Soc.*, **157**, A1212 (2010).
9. F. Sagane, R. Shimokawa, H. Sano, H. Sakaebe, and Y. Iriyama, *J. Power Sources*, **225**, 245 (2013).
10. C. Brissot, M. Rosso, J.-N. Chazalviel, P. Baudry, and S. Lascaud, *Electrochim. Acta*, **43**, 1569 (1998).
11. J. K. Stark, Y. Ding, and P. A. Kohl, *J. Electrochem. Soc.*, **160**, D337 (2013).
12. K. Nishikawa, T. Mori, T. Nishida, Y. Fukunaka, and M. Rosso, *J. Electroanal. Chem.*, **661**, 84 (2011).
13. T. Hirai, I. Yoshimatsu, and J. Yamaki, *J. Electrochem. Soc.*, **141**, 611 (1994).
14. K. Kanamura, S. Shiraishi, and Z. Takehara, *J. Electrochem. Soc.*, **143**, 2187 (1996).
15. S. Shiraishi, K. Kanamura, and Z. Takehara, *J. Appl. Electrochem.*, **29**, 869 (1999).
16. D. Aurbach, E. Zinigrad, H. Teller, Y. Cohen, G. Salitra, H. Yamin, P. Dan, and E. Elster, *J. Electrochem. Soc.*, **149**, A1267 (2002).
17. Y. Gofer, M. Ben-Zion, and D. Aurbach, *J. Power Sources*, **39**, 163 (1992).
18. F. Ding, W. Xu, G. L. Graff, J. Zhang, M. Sushko, X. Chen, Y. Shao, M. H. Engelhard, Z. Nie, J. Xiao, X. Liu, P. V Sushko, J. Liu, and J.-G. Zhang, *J. Am. Chem. Soc.*, (2013).
19. J. K. Stark, Y. Ding, and P. A. Kohl, *J. Electrochem. Soc.*, **158**, A1100 (2011).
20. R. Wibowo, L. Aldous, S. E. W. Jones, and R. G. Compton, *Chem. Phys. Lett.*, **492**, 276 (2010).
21. D. Aurbach, Y. Gofer, Z. Lu, a. Schechter, O. Chusid, H. Gizbar, Y. Cohen, V. Ashkenazi, M. Moshkovich, and R. Turgeman, *J. Power Sources*, **97-98**, 28 (2001).
22. Z. Feng, Y. NuLi, J. Wang, and J. Yang, *J. Electrochem. Soc.*, **153**, C689 (2006).
23. D. Aurbach, H. Gizbar, A. Schechter, O. Chusid, H. E. Gottlieb, Y. Gofer, and I. Goldberg, *J. Electrochem. Soc.*, **149**, A115 (2002).
24. J. Muldoon, C. B. Bucur, A. G. Oliver, T. Sugimoto, M. Matsui, H. S. Kim, G. D. Allred, J. Zajicek, and Y. Kotani, *Energy Environ. Sci.*, **5**, 5941 (2012).
25. Y. NuLi, J. Yang, and R. Wu, *Electrochem. Commun.*, **7**, 1105 (2005).
26. O. Shimamura, N. Yoshimoto, M. Matsumoto, M. Egashia, and M. Morita, *J. Power Sources*, **196**, 1586 (2011).
27. S. Joseph and P. V. Kamath, *J. Electrochem. Soc.*, **153**, D99 (2006).
28. B. E. Prasad and P. V. Kamath, *Bull. Mater. Sci.*, **36**, 475 (2013).
29. S. Joseph, S. Upadhya, and P. V. Kamath, *J. Chem. Sci.*, **121**, 685 (2009).
30. J. Katić, M. Metikoš-Huković, and R. Babić, *J. Appl. Electrochem.*, In press (2013).
31. H. Sakaebe, H. Matsumoto, and K. Tatsumi, *Electrochim. Acta*, **53**, 1048 (2007).
32. C. Scordilis-kelley and R. T. Carlin, *J. Electrochem. Soc.*, **140**, 1606 (1993).
33. R. Wibowo, L. Aldous, E. I. Rogers, S. E. W. Jones, and R. G. Compton, *J. Phys. Chem. C*, **114**, 3618 (2010).
34. J. a. Vega, J. Zhou, and P. a. Kohl, *J. Electrochem. Soc.*, **156**, A253 (2009).
35. C. Scordilis-kelley, J. Fuller, and R. T. Carlin, *J. Electrochem. Soc.* **139**, 694 (1992).
36. J. O. Besenhard, ed., *Handbook of Battery Materials*, Wiley-VCH, New York, 1999.
37. J. K. Stark, Y. Ding, and P. A. Kohl, *J. Phys. Chem. C*, **117**, 4980 (2013).
38. A. A. Kornyshev, *J. Phys. Chem. B*, **111**, 5545 (2007).
39. M. V. Fedorov and A. a. Kornyshev, *Electrochim. Acta*, **53**, 6835 (2008).
40. K. Kirchner, T. Kirchner, V. Ivanišťšev, and M. V. Fedorov, *Electrochim. Acta* (2013).
41. M. Z. Bazant, B. D. Storey, and A. a. Kornyshev, *Phys. Rev. Lett.*, **106**, 046102 (2011).